Chinese Journal of Aeronautics, (2014),27(6): 1619–1624

Chinese Society of Aeronautics and Astronautics
& Beihang University

Chinese Journal of Aeronautics

cja@buaa.edu.cn
www.sciencedirect.com

Characteristics of motorized spindle supported by active magnetic bearings

Xie Zhenyu [a,b,*], Yu Kun [a], Wen Liantang [c], Wang Xiao [a], Zhou Hongkai [a]

[a] Department of Design Engineering, Nanjing University of Aeronautics and Astronautics, Nanjing 210016, China
[b] Jiangsu Key Laboratory of Precision and Micro-Manufacturing Technology, Nanjing 210016, China
[c] Jiangxi Zhonghang Optics Equipment Co. Ltd., Jingdezhen 333000, China

Received 22 April 2014; revised 27 May 2014; accepted 3 September 2014
Available online 18 October 2014

KEYWORDS

Dynamic characteristics;
Finite element analysis;
Loss;
Magnetic bearings;
Modal analysis;
Spindle design

Abstract A motorized spindle supported by active magnetic bearings (AMBs) is generally used for ultra-high-speed machining. Iron loss of radial AMB is very great owing to high rotation speed, and it will cause severe thermal deformation. The problem is particularly serious on the occasion of large power application, such as all electric aero-engine. In this study, a prototype motorized spindle supported by five degree-of-freedom AMBs is developed. Homopolar and heteropolar AMBs are independently adopted as radial bearings. The influences of the two types of radial AMBs on the dynamic characteristics of the motorized spindle are comparatively investigated by theoretical analysis, test modal analysis and actual operation of the system. The iron loss of the two types of radial AMBs is analyzed by finite element software and verified through run-down experiments of the system. The results show that the structures of AMB have less influence on the dynamic characteristics of the motorized spindle. However, the homopolar structure can effectively reduce the iron loss of the radial AMB and it is useful for improving the overall performance of the motorized spindle.

1. Introduction

Worldwide, ultra-high-speed machining technology, which has much high cutting and feeding speed than the conventional, is recognized as one of four major advanced manufacturing technologies. A motorized spindle combines motor shaft and machine tool principal axis without belt and gear transmission and it is the most critical component of ultra-high-speed machining equipment. Generally, the motorized spindle is supported by ball bearings.[1]

Unlike ball bearing, active magnetic bearing (AMB) does not suffer from mechanical contact and wear, has less noise, does not require any lubricant and sealing, and is characterized by long service life.[2,3] A motorized spindle with AMBs features adjustable support stiffness and damping, high rotation precision, and easy real-time monitoring. Owing to the above assets, AMB can also be applied to aero-engine.[4]

* Corresponding author. Tel.: +86 25 81034135.
E-mail address: xiezy@nuaa.edu.cn (Z. Xie).

Peer review under responsibility of Editorial Committee of CJA.

Production and hosting by Elsevier

http://dx.doi.org/10.1016/j.cja.2014.10.031

To improve the dynamic characteristics of motorized spindle, many new control strategies for AMB have been proposed.[5–8] Furthermore, motorized spindle suffers from a problem that the large temperature rise can cause severe thermal deformation and thus reduce machining accuracy.

Miroslaw et al.,[9] utilized infrared camera images to identify major heat sources in the machine tool and they evaluated the thermal expansion of the machine by means of finite element analysis. Tamura et al.,[10] developed a motorized spindle with a self-cooling function and used rotational experiments to demonstrate that it could minimize the thermal deformation. Zhang and Li[11] used finite element analysis to simulate the temperature field, steady-state temperature distribution, transient temperature distribution and thermal error of a spindle system. Uhlmann and Hu[12] presented a 3D finite element model to predict the thermal behavior of a high-speed motor spindle. Li and Zhao[13] effectively reduced the axial thermal error at varying spindle speeds by compensating the thermal error using predicted data. Sheng et al.[14] analyzed the steady temperature field and the thermal deformation of the spindle and they proposed a solution to install a cooling sleeve in front of the spindle box, which can apparently reduce the thermal error of the spindle. Zhang et al.,[15] adopted a serial and a parallel grey neural network to predict the thermal error and they validated their method through experiments on the spindle deformation in the axial direction on a five-axis machining center. Horiuchi et al.[16] analyzed the influence of the thermal behavior of the spindle on the machining accuracy in micro-endmilling. Lu et al.[17] established a finite element model of the thermal characteristics of a motorized spindle and studied the distribution of the spindle steady-state temperature field and effect of spindle speed and bearing lubrication on the thermal deformation of the spindle. Li et al.[18] developed a prototype motorized spindle supported by five degree-of-freedom AMBs, investigated the relationship between temperature rise, grinding head posture and the controller's five reference inputs, discovered the serious effect of the temperature rise on the precision of grinding and introduced online adjustment of the grinding head posture and automatic thermal expansion compensation into the system. Wu and Hu[19] analyzed the temperature field of a magnetically levitated grinding spindle by finite element software, adopted a thermal infrared imager to measure the temperature field distribution and mentioned the importance of thermal design and structural design on the temperature distribution of the system.

A motorized spindle supported by AMBs has two internal heat sources: AMBs and the built-in motor.[20] The surface eddy current and hysteresis loss of AMBs are important factors in temperature increase. The problem is particularly serious on the occasion of large power application, such as all electric aero-engine. Therefore, it is essential to investigate approaches by which the surface eddy current and hysteresis loss of AMBs can be reduced. In this study, heteropolar and homopolar AMB are developed for motorized spindle respectively. The influences of the two types of radial AMBs on the dynamic characteristics of the motorized spindle are comparatively investigated by theoretical analysis, test modal analysis and actual operation of the system. The iron loss of the two types of radial AMBs is also analyzed by ANSOFT MAXWELL 3D software and verified through run-down experiments of the system.

2. Test device

Fig. 1 shows the mechanical structure of the motorized spindle prototype. The rotor (working speed: 60000 r/min) is supported by two radial AMBs and one axial AMB and it is driven by a built-in motor (power: 1 kW). Rotor vibrations can be detected in real-time by five pairs of differential displacement sensors.

Generally, a radial AMB has a heteropolar structure, i.e., the N and S poles are cross-arranged along the circumferential direction. When the rotor completes a revolution, the magnetic line of force reverses several times at the same position on the rotor surface. Although a lamination-type stator and rotor are generally used, the surface eddy current and hysteresis loss are still obvious and serious. The situation is different in a homopolar structure, in which each pair of magnetic poles is distributed along the axial direction and only N or S poles are located along the circumferential direction, without reversing the magnetic line of force; therefore, the surface eddy current and hysteresis loss are slight and little, respectively, and only the machining process becomes slightly more complicated.

Fig. 2 shows the structures of homopolar and heteropolar AMBs, respectively. According to the design of the structure parameter, the nominal air gap C_{r0}, bias current I_{r0} and maximum electromagnetic force F_{rmax} of the two types of radial AMBs are 0.2 mm, 2.5 A, and 20 N, respectively. For the axial AMB, the corresponding values are 0.2 mm, 2.5 A and 50 N; furthermore, the rotor length l is 218 mm, symmetry center distance of the two radial AMBs l_1 is 127 mm and two ball bearings are used as protective bearings.

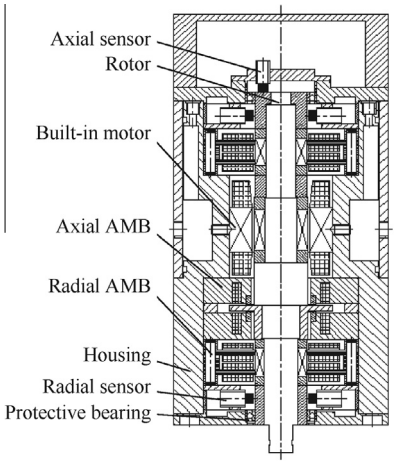

Fig. 1 Mechanical structure of motorized spindle.

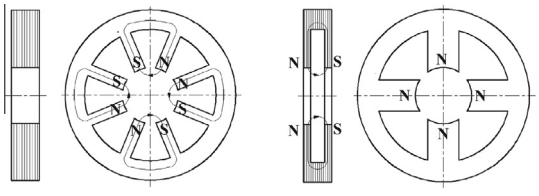

Fig. 2 Schematic diagram of AMB.

3. Theoretical analysis

In consideration of the fact that the lateral vibration of the rotor is the main factor influencing the dynamic characteristics of a bearing-rotor system, the rotor axial degree of freedom can be ignored in the theoretical analysis.

The controller adopts incomplete differential PID (proportion–integral–derivative) strategies and its transfer function can be expressed as

$$G_c(s) = k_p + \frac{k_i}{s} + \frac{k_d s}{1 + T_d s} \tag{1}$$

where k_p, k_i, k_d, and T_d denote proportional coefficient, integral coefficient, differential coefficient, and differential time coefficient, respectively.

The rotor is simplified as a node model with 44 lumped masses and lumped rotating inertia. Each node is connected via different cross shaft sections without mass. The radial AMBs are respectively located at the 11th and 38th nodes. $\bar{x}$, $\bar{y}$, $\bar{\varphi}$ and $\bar{\psi}$ respectively denote the non-dimensional linear displacement and angular displacement of each node, $\bar{i}_x$ and $\bar{i}_y$ respectively denote the non-dimensional control current of the AMBs in the x and y directions. According to the lumped parameter method, the dimensionless system equation can be expressed as follows:

$$\begin{bmatrix} 0 & \bar{\boldsymbol{M}} & 0 \\ \bar{\boldsymbol{M}} & \bar{\boldsymbol{C}} & 0 \\ \bar{\boldsymbol{K}}_{z1} & \bar{\boldsymbol{K}}_{z2} & \bar{\boldsymbol{K}}_{z3} \end{bmatrix} \dot{\boldsymbol{R}} + \begin{bmatrix} \bar{\boldsymbol{M}} & 0 & 0 \\ 0 & \bar{\boldsymbol{K}} & \bar{\boldsymbol{K}}_{zi} \\ 0 & \bar{\boldsymbol{K}}_{z4} & \bar{\boldsymbol{K}}_{z5} \end{bmatrix} \boldsymbol{R} = \boldsymbol{0} \tag{2}$$

where $\bar{\boldsymbol{M}}$, $\bar{\boldsymbol{C}}$ and $\boldsymbol{R}$ denote the mass matrix, damping matrix and state variable. $\bar{\boldsymbol{K}}_{z1}$, $\bar{\boldsymbol{K}}_{z2}$, $\bar{\boldsymbol{K}}_{z3}$, $\bar{\boldsymbol{K}}_{z4}$, $\bar{\boldsymbol{K}}_{z5}$ and $\bar{\boldsymbol{K}}_{zi}$ denote the related stiffness matrices, respectively.

The state variable $\boldsymbol{R}$ can be expressed as

$$\boldsymbol{R}^{\mathrm{T}} = [\boldsymbol{R}_1, \boldsymbol{R}_2, \boldsymbol{R}_3] \tag{3}$$

Therefore,

$$\boldsymbol{R}_1^{\mathrm{T}} = \left[\dot{\bar{x}}_1, \dot{\bar{y}}_1, \dot{\bar{\varphi}}_1, \dot{\bar{\psi}}_1, \dot{\bar{x}}_2, \dot{\bar{y}}_2, \dot{\bar{\varphi}}_2, \dot{\bar{\psi}}_2, \ldots, \dot{\bar{x}}_{44}, \dot{\bar{y}}_{44}, \dot{\bar{\varphi}}_{44}, \dot{\bar{\psi}}_{44}\right],$$
$$\boldsymbol{R}_2^{\mathrm{T}} = \left[\bar{x}_1, \bar{y}_1, \bar{\varphi}_1, \bar{\psi}_1, \bar{x}_2, \bar{y}_2, \bar{\varphi}_2, \bar{\psi}_2, \ldots, \bar{x}_{44}, \bar{y}_{44}, \bar{\varphi}_{44}, \bar{\psi}_{44}\right],$$
$$\boldsymbol{R}_3^{\mathrm{T}} = \left[\dot{\bar{i}}_{x1}, \dot{\bar{i}}_{y1}, ,\bar{i}_{x1}, \bar{i}_{y1}, \dot{\bar{i}}_{x2}, \dot{\bar{i}}_{y2}, ,\bar{i}_{x2}, \bar{i}_{y2}\right]$$

where the subscript 1, 2, … , 44 denote the serial numbers of the rotor nodes, and the subscript $x1$, $y1$, $x2$ and $y2$ denote the four freedoms of the radial AMB.

By Eq. (2), it is possible to obtain the stable region of the AMB control parameters, system eigenvalues and eigenvectors under specific AMB control parameters and rotation speeds. These results, in turn, enable further calculation of the natural frequencies and mode shapes in various orders.

According to the stable region of the control parameters, for the radial AMBs, k_p, k_i, k_d, and T_d are respectively selected as 2.26, 14.0, 1.3×10^{-3}, and 1.12×10^{-5} s. According to a self-developed Matlab program, the rotor mode shapes in the first three orders can be calculated as shown in Fig. 3 and the corresponding natural frequencies are shown in Table 1.

Fig. 3 and Table 1 show that the motorized spindle prototype has two types of rigid natural frequencies in translational and conical vibration. The 1st-order bending natural frequency is approximately 1.5 times more than the working speed, and higher-order natural frequencies cannot be considered owing to the high deviation from the working speed.

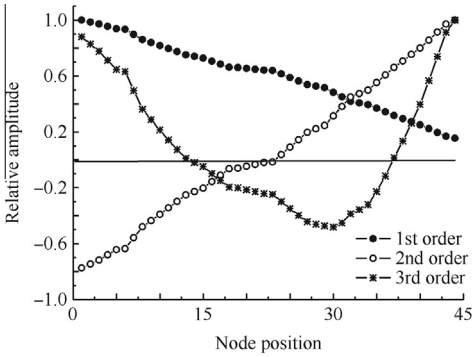

Fig. 3 First three mode shapes of rotor.

Table 1 Natural frequency and mode shape of system.

Order	Natural frequency (Hz)	Mode shape
1st	45.0	Translational
2nd	73.8	Conical
3rd	1498.3	1st-order bending

In addition, it is shown from the mathematical model that when the nominal air gap C_{r0}, bias current I_{r0} and maximum electromagnetic force F_{rmax} are equal, both heteropolar and homopolar radial AMBs have the same current and displacement stiffness coefficient; if the control parameters are also the same, the supporting features of the two types of radial AMBs are exactly consistent, which will not affect the results of theoretical analysis.

4. Test modal analysis

Test modal analysis is mainly applied to predicting the running performance of the motorized spindle prototype at high speed. The general steps involved are as follows: suspend the motorized spindle rotor stably, knock the lower end of the rotor (where the grinding wheel is mounted) with a modal hammer, record the system response in a given frequency band using a piezoelectric acceleration sensor and analyze the system's natural frequency and modal damping according to the output of the modal hammer and piezoelectric acceleration sensor. Only the lower end of the rotor is exposed and the rest of it is enclosed by the motorized spindle housing; therefore, it is impossible to determine the mode shape of the rotor through test modal analysis.

The radial AMBs respectively adopt heteropolar and homopolar structures, the control parameters of which are as mentioned above; k_p, k_i, k_d and T_d for the axial AMBs are respectively selected as 1.98, 12.23, 2.3×10^{-3}, and 1.12×10^{-5} s. Under the AMB's action, the rotor can be stably suspended. The test equipment used is French OROS's OR34 four-channel dynamic signal test and analysis instrument, a PCB hammer and ICP accelerometer. When the radial AMB has a heteropolar structure, the test results of the system frequency response function are as shown in Fig. 4. For the radial AMB with homopolar structure, the

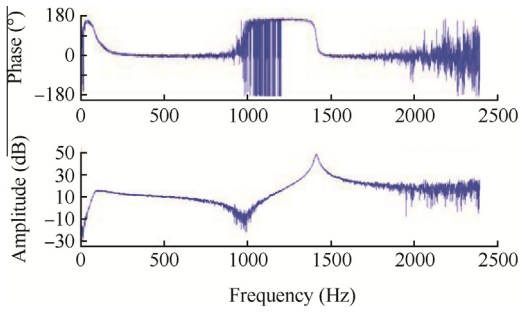

Fig. 4 System frequency response function by hammer method.

test results of the system frequency response function are similar to the data shown in Fig. 4.

After the analysis of the system frequency response function using N-Modal modal analysis software, which is developed by the Dynamic Test and Analysis Center at Nanjing University of Aeronautics and Astronautics, the first two order natural frequencies and modal dampings of the system can be obtained. For the radial AMB with heteropolar structure, the first two order natural frequencies of the system are 100.3 Hz and 1411.3 Hz, respectively, and the modal dampings corresponding to the natural frequencies are 33.3% and 0.87%. While for the radial AMB with homopolar structure, the first two order natural frequencies of the system are 80.4 Hz and 1423.2 Hz respectively, and the modal dampings corresponding to the natural frequencies are 46.8% and 1.27%.

The results above show that the motorized spindle prototype has two orders of natural frequencies within 2500 Hz, wherein modal damping corresponding to the 1st-order natural frequency is higher.

Based on the theoretical analysis and test modal analysis results, the following conclusions can be drawn: the motorized spindle rotor can be regarded as a rigid rotor within the working speed range; the translational or conical modal vibration of the rotor does not appear in test modal analysis because the corresponding modal damping is too large; the two structures of radial AMBs do not significantly impact the natural frequencies and modal damping of the system.

5. High-speed rotation experiment

Fig. 5 shows a photogragh of the motorized spindle prototype. It consists of a mechanical device and AMB electronic control system (including sensor, controller, power amplifier and power supply module) as well as a high-frequency power supply for driving the built-in motor.

The AMB control parameters are as described previously. The radial AMB respectively adopts heteropolar and homopolar structures; furthermore, the rotor is stably suspended by AMBs and rotates at the working speed of the built-in motor.

The sensitivity of the differential displacement sensor is 6×10^{-5} m/V. When the system is running, the output of the radial differential displacement sensor 33 mm away from the lower end of rotor is sent to the HP35670A dynamic signal analyzer for further spectrum analysis; therefore, the radial vibration amplitude S of the rotor can be obtained in real-time with the rotation speed n at this position, as shown in Fig. 6.

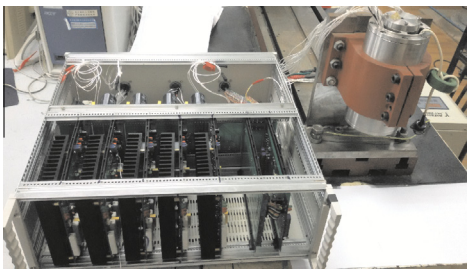

Fig. 5 Prototype of motorized spindle system.

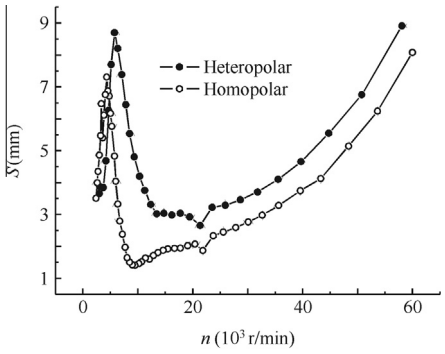

Fig. 6 Vibration amplitude of rotor at run time.

Fig. 6 shows that regardless of whether the AMBs are heteropolar or homopolar, the system can run at speeds up to 60000 r/min. When heteropolar or homopolar radial AMBs are used, the system vibration peaks at 5760 and 4320 r/min, respectively. Within the scope of rotation speed from 20000 to 60000 r/min, the vibration amplitude of the rotor increases with the speed. The vibration amplitude of the rotor for the homopolar radial AMB is slightly lower than that of the heteropolar radial AMB.

6. Iron loss of radial AMB

The iron loss of a radial AMB contains the eddy current and hysteresis loss, which results from magnetic field transformation in the iron cores, and is related to the changing frequency, i.e., control current frequency of the magnetic field.

Firstly, ANSOFT MAXWELL 3D software is adopted to analyze the iron loss of the two types of AMBs. Fig. 7 shows 3D finite element models of the two types of AMBs.

Assuming that an unbalanced mass is the only exciting source, the frequencies of the rotor vibration and the control current of the AMB are the same as the rotation speed. If the control current amplitude is 2.5 A, by the finite element calculation, the iron loss P of the two types of radial AMBs is as shown in Fig. 8.

Fig. 8 shows that for both types of radial AMBs, the iron loss increases with the rotor speed, while at the same speed, iron loss of homopolar radial AMB is significantly lesser than heteropolar radial AMB.

If the built-in motor is powered off, when the rotor rotates at the working speed, the rotor speed is gradually reduced to

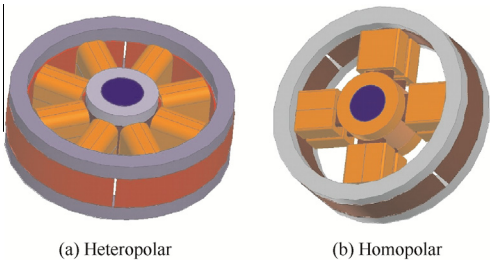

Fig. 7 3D models of radial AMB structure.

zero (free run-down), and all of the kinetic energy is dissipated in the form of air friction loss of the rotor and iron loss of the AMBs. Therefore, relevant data about the iron loss of AMBs can be obtained through a run-down experiment.

The AMB control parameters are as described previously. The radial AMBs respectively adopt heteropolar and homopolar structures. The rotor is suspended stably and runs at up to 60000 r/min. Then the built-in motor is powered off and the rotor speed gradually reduces to zero. In the run-down process, the curve of the rotor speed versus time is shown in Fig. 9.

In the run-down process, the energy and power of the rotor are respectively calculated by Eqs. (4) and (5).

$$E_k = \frac{1}{2} J_p \omega^2 \tag{4}$$

$$P_k = \frac{dE_k}{dt} = J_p \omega \frac{d\omega}{dt} + \frac{\omega^2}{2} \frac{dJ_p}{dt} = J_p \omega \frac{d\omega}{dt} \tag{5}$$

where E_k, P_k and ω denote the energy, power and angular speed of the rotor, and the moment of inertia J_p is $0.000184\ \mathrm{kg \cdot m^2}$.

By Eq. (5), according to the curve of the rotor speed versus time, the total power loss in the form of air friction loss of the rotor and iron loss of the AMBs at different speeds can be calculated (see Fig. 10).

The difference between the two curves in Fig. 10 indicates the power saving under the homopolar structure, assuming that the air friction losses of the rotor are similar during the run-down process when heteropolar or homopolar radial AMBs are adopted separately. Fig. 10 shows that as the rotor speed increases, the homopolar structure more obviously influences the reduction in the eddy current and hysteresis loss of the radial AMB. In addition, the difference between the two curves in Fig. 10 is larger than that in Fig. 8, because the real control current contains many parts with different frequencies.

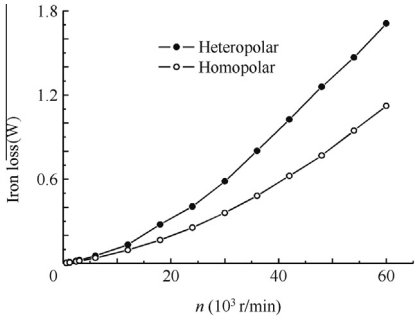

Fig. 8 Iron loss of AMB at different speeds of rotor.

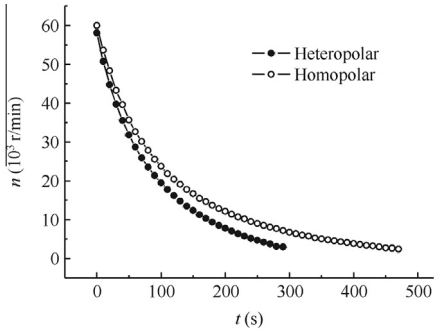

Fig. 9 Curve of rotor speed versus time in run-down process.

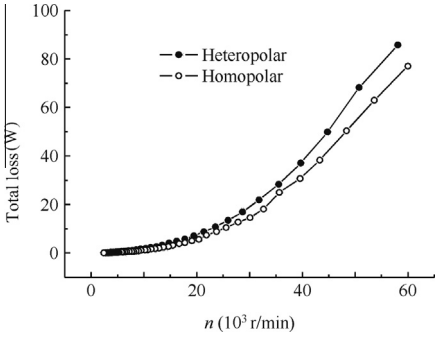

Fig. 10 Total power loss of AMB at different speeds.

7. Conclusions

(1) When a heteropolar or homopolar radial AMB is adopted, the motorized spindle prototype can stably run at up to 60000 r/min.

(2) Regardless of whether heteropolar or homopolar radial AMB is used, the motorized spindle prototype has two types of rigid modes, translational and conical mode in the low-frequency band, and both the corresponding modal dampings are higher. The 1st-order bending natural frequency is more than 1400 Hz and the motorized spindle rotor can be regarded as a rigid rotor within the working speed range.

(3) Both heteropolar and homopolar AMB structure have no significant influence on the dynamic characteristics of the motorized spindle prototype.

(4) For both heteropolar and homopolar radial AMBs, the iron loss increases with the rotor speed. However, at the same speed, iron loss of homopolar radial AMB is significantly lesser than heteropolar radial AMB; this is helpful in reducing the temperature rise and improving the overall characteristics of motorized spindle.

(5) Compared with heteropolar radial AMB, homopolar radial AMB is suitable for motorized spindle. It would be highly advantageous to apply homopolar radial AMB on the occasion of large power, such as all electric aero-engine.

Acknowledgements

This study was co-supported by the National Natural Science Foundation of China (No. 51275238) and a Project Funded by Priority Academic Program Development of Jiangsu Higher Education Institutions (PAPD) of China.

References

1. Jedrzejewski J, Kwasny W. Modelling of angular contact ball bearings and axial displacements for high-speed spindles. *CIRP Ann – Manuf Technol* 2010;**59**(1):377–82.
2. Xie ZY, Long YW, Xu X. Experimental investigation for dynamic characteristics of the active magnetic bearing rotor system with zero Bias Current. *J Mech Eng* 2013;**49**(15):68–73 [Chinese].
3. Xie ZY, Wang X, Zhou HK. Supporting characteristics of the homopolar active magnetic bearing for wind power generator. *J Vib Eng* 2013;**26**(1):112–7 [Chinese].
4. Wang GY. Study of a more-electric engine with active magnetic bearings. *Gas Turbine Exp Res* 2007;**20**(4):15–8 [Chinese].
5. Lee RM, Tsai NC. Anti-windup embedded magnetic actuator applied for near-high-speed milling. *Int J Adv Manuf Technol* 2013;**64**(5–8):669–79.
6. Madden RJ, Sawicki JT. Rotor model validation for an active magnetic bearing machining spindle using mu-synthesis approach. *J Eng Gas Turbines Power* 2012;**134**(9):1–6.
7. Gourc E, Seguy S, Arnaud L. Chatter milling modeling of active magnetic bearing spindle in high-speed domain. *Int J Mach Tools Manuf* 2011;**51**(12):928–36.
8. Kimman MH, Langen HH, Munnig RH. A miniature milling spindle with active magnetic bearings. *Mechatronics* 2010;**20**(2):224–35.
9. Miroslaw P, Henryk M, Jacek Z. Examination of thermal deformation of micro milling machine tool SNTM-CM-ZUT-1. *Diagnostyka* 2013;**14**(1):31–6.
10. Tamura Y, Sawano H, Yoshioka H, Shinno H. A thermally stable high speed spindle system equipped with self-cooling function. *Key Eng Mater* 2012;**523–524**:527–31.
11. Zhang JB, Li HW. Thermal performance analysis for the machine tool's spindle. *Proceedings of the 2012 7th IEEE Conference on Industrial Electronics and Applications*; 2012. p. 2131–34.
12. Uhlmann E, Hu J. Thermal modelling of a high speed motor spindle. *Proceedings of the 5th CIRP Conference on High Performance Cutting*; 2012. p. 313–8.
13. Li Y, Zhao WH. Axial thermal error compensation method for the spindle of a precision horizontal machining center. *Proceedings of 2012 IEEE International Conference on Mechatronics and Automation*; 2012. p. 2319–23.
14. Sheng ZQ, Zhu ZX, Liu CC, Zhang CB. Research on thermal characteristic of spindle system of CNC machine tool. *Adv Mater Res* 2012;**510**:23–7.
15. Zhang Y, Yang JG, Jiang H. Machine tool thermal error modeling and prediction by grey neural network. *Int J Adv Manuf Technol* 2012;**59**(9–12):1065–72.
16. Horiuchi O, Nomura M, Ma BX, Shibata T, Murakami Y, Masuda M. Influence of thermal behavior of spindle on machining accuracy in micro-endmilling. *Adv Mater Res* 2012;**418–420**:2040–5.
17. Lu Y, Gao SD, Hao ZP. Study on steady-state temperature field and thermal deformation for permanent magnet synchronous motorized spindle. *Adv Mater Res* 2011;**305**:340–3.
18. Li DG, Liu SQ, Bian B. Automatic thermal expansion compensation of the precise grinding machine AMB spindle. *Appl Mech Mater* 2012;**130–134**:3221–4.
19. Wu HC, Hu YF. Thermal characteristics of magnetic levitated grinding spindle. *J Mech Eng* 2010;**46**(20):9–33 [Chinese].
20. Xu X. Dynamic characteristics of low loss motorized spindle suspended by magnetic bearings dissertation. Nanjing: Nanjing University of Aeronautics and Astronautics; 2012. [Chinese].

Xie Zhenyu received M.S. degree from Xi'an University of Technology in 1997 and Ph.D. degree from Xi'an Jiaotong University in 2000. He is currently an associated professor at Department of Design Engineering, Nanjing University of Aeronautics and Astronautics, China. His main research interests include dynamic analysis, test modal analysis and control theory on AMB.